https://ajeat.org/ ISSN: XXXX - XXXX

Academic Journal of Engineering Applications (AJEA)
Volume: 1 Issue: 1, July 2026, pp. 38 – 51

Predictive control of temperature in hydroponic systems

Rahma Boughamoura, Maher Ben Hariz, Faouzi Bouani
University of Tunis El Manar,
National Engineering School of Tunis,
LR11ES20 Laboratory of Analysis, Design and Control of Systems,
P.O. Box 37, 1002 Belvedere, Tunis, Tunisia
rahma.boughamoura@etudiant-enit.utm.tn, maher.benhariz@enit.utm.tn, faouzi.bouani@enit.utm.tn

Abstract— Hydroponic cultivation requires precise control of environmental factors to optimize plant growth and resource eff iciency. Among these factors, temperature plays a crucial role in plant metabolism, nutrient absorption, and overall system stability. This work presents the design and experimental evaluation of an automatic temperature regulation system for hydroponic applications. Two control strategies are implemented and compared: a Proportional-Integral (PI) controller and a predictive control approach. The results demonstrate the effectiveness of both methods in maintaining the desired temperature despite disturbances, with improved performance observed using predictive control.

Keywords— Hydroponics, Temperature Regulation, PI Controller, Predictive Control, ESP32

I. INTRODUCTION

Hydroponic agriculture has emerged as a promising alternative to conventional soil-based farming in response to global challenges such as population growth, land scarcity, and climate variability. Hydroponics refers to a cultivation technique where plants grow without soil, receiving essential nutrients through an aqueous nutrient solution supplied directly to their roots. This approach enables crops to be produced in controlled environments where parameters such as nutrient concentration, temperature, humidity, and light can be precisely managed. Such control improves production eff iciency and allows cultivation in regions with poor soil quality or limited agricultural land [1], [3], [17]. Moreover, hydroponic systems can significantly enhance land-use eff iciency and allow vertical or indoor farming configurations, making them particularly suitable for urban agriculture and controlled-environment agriculture [1], [2]. Among the various environmental factors affecting plant growth, temperature plays a fundamental role. Temperature influences plant metabolic rates, enzymatic activity, nutrient uptake, and the balance between respiration and photosynthesis, which directly determines overall growth and yield in hydroponic systems [5], [6]. In hydroponically cultivated plants, temperature affects both the aerial environment and the nutrient solution, where deviations from optimal thermal conditions can reduce biomass production, alter nutrient availability, and trigger stress responses that negatively impact crop quality [7], [8]. Maintaining an optimal thermal environment is therefore essential for vigorous development and eff icient physiological functioning in controlled agriculture.

Experimental studies have shown that temperature variations strongly influence growth performance, root morphology, and crop susceptibility to disease in hydroponic systems. For example, Rathedi *et al.* demonstrated that precise temperature control significantly improves system stability and crop performance compared to uncontrolled thermal conditions [6]. Similarly, Wahyuni *et al.* implemented automated temperature regulation using PID control and showed that maintaining temperature setpoints within narrow bounds enhances plant metabolic eff iciency and reduces thermal stress [7]. Furthermore, advanced hybrid control techniques such as adaptive Dung Beetle Optimizer–fuzzy PID have been applied to nutrient solution temperature control, revealing enhanced adaptability and reduced steady-state errors compared to classical controllers [8].

In hydroponic agriculture, plants require precise and dynamic temperature control because optimal thermal requirements vary depending on species, developmental stage, and environmental conditions. Thermal fluctuations can inhibit enzymatic processes, slow growth rates, and decrease nutrient uptake eff iciency, while excessively high temperatures can lead to heat stress, reduced photosynthetic capacity, and accelerated respiration losses [5], [6]. Consequently, maintaining appropriate temperature levels is essential to ensure both crop productivity and energy eff iciency in

Submitted - May 2026; Final Version Received – July 2026; Accepted - July 2026; Published Online – July 2026

https://ajeat.org/ ISSN: XXXX - XXXX

Academic Journal of Engineering Applications (AJEA)
Volume: 1 Issue: 1, July 2026, pp. 38 – 51

controlled agricultural systems. Traditionally, temperature regulation in hydroponic systems has been achieved using simple thermostat mechanisms, fixed schedules, or manual adjustments. While these methods are straightforward, they often fail to maintain stable and optimal temperature levels in the presence of disturbances or environmental variations. The integration of classical control strategies such as PI and predictive control considerably improves thermal stability, energy eff iciency, and overall system performance [7], [9].

Recent advancements have introduced intelligent and model-based temperature control strategies. Model Predictive Control (MPC) approaches, for example, have been extensively reviewed for greenhouse and controlled environment applications, showing superior disturbance rejection and setpoint tracking compared to classical PID or PI controllers [9], [10]. Hamidane *et al.* applied constrained discrete MPC to greenhouse temperature regulation and achieved tighter control of thermal variables under external perturbations, highlighting the potential of predictive strategies in dynamic environments [11]. These predictive methods can incorporate constraints, anticipate future thermal variations, and optimize control actions, making them suitable for more demanding hydroponic temperature control tasks.

In this context, the objective of this work is to design and implement an automatic temperature regulation system for hydroponic cultivation using classical and advanced control strategies, including Proportional-Integral (PI) and predictive control. The proposed approach aims to dynamically adjust the thermal environment based on real-time feedback from temperature sensors to maintain the desired setpoints required for optimal plant growth, while ensuring eff icient energy usage. The study focuses on experimental implementation and performance evaluation of these control algorithms in a hydroponic cultivation setup. The remainder of this paper is organized as follows. The second section presents the control strategies, where the predictive approach and the PI controller are introduced. The third section describes the system under study and details the parameter identification of the mathematical model. The fourth section presents the experimental results and their discussion. Finally, the paper concludes with a summary of the main findings.

II. CONTROL STRATEGIES

In this work, two control strategies are implemented to regulate the temperature of the system: a Proportional-Integral (PI) controller and a predictive control approach. The objective is to ensure that the measured temperature accurately tracks the desired reference temperature.

A. PI Controller

The Proportional-Integral (PI) controller is one of the most widely used control strategies due to its simplicity and effectiveness in eliminating steady-state error. It is based on proportional and integral actions and is particularly suitable for temperature regulation systems, which typically exhibit slow dynamics.

In continuous time, the control law is expressed as:

$$u(t) = K_p e(t) + K_i \int_0^t e(\tau) d\tau \qquad (1)$$

For digital implementation on the ESP32, the controller is discretized. Using a backward Euler approximation, the discrete-time form becomes:

$$u(k) = u(k-1) + c_0 e(k) + c_1 e(k-1) \qquad (2)$$

where $u(k)$ is the control signal applied to the AC dimmer and c_0, c_1 are the PI controller parameters.

The proportional term provides a fast response to variations in temperature error, while the integral term eliminates steady-state error by accumulating past deviations. This makes the PI controller effective for maintaining a stable thermal environment.

However, due to the high thermal inertia of the system (heater and enclosure), the system is characterized by slow dynamic behavior, leading to a delayed response and possible overshoot if the controller is not properly tuned.

Submitted - May 2026; Final Version Received – July 2026; Accepted - July 2026; Published Online – July 2026

B. Predictive controller

a) CARIMA Model: The CARIMA (Controlled Auto-Regressive Integrated Moving Average) model describes system dynamics while ensuring zero steady-state error through integration. The output is given by:

$$y(k) = \frac{q^{-1}B(q^{-1})}{A(q^{-1})}\,u(k) + \frac{1}{A(q^{-1})\,\Delta}\,v(k) \tag{3}$$

where:

- $y(k)$ is the system output, $u(k)$ is the control input,
- $v(k)$ is a noise sequence, $\Delta = 1 - q^{-1}$,
- $A(q^{-1}) = 1 + a_1 q^{-1} + \cdot\cdot\cdot + a_{nA} q^{-n_A}$,
- $B(q^{-1}) = b_0 + b_1 q^{-1} + \cdot\cdot\cdot + b_{nB} q^{-n_B}$.

The noise signal $v(k)$ is assumed to be a zero-mean white noise with finite variance.

From the CARIMA model formulation, it is possible to derive the j-step ahead predictor of the system output, which is a key element in predictive control design.

b) The j-step ahead predictor: From the CARIMA model in (3), the j-step ahead predictor is given by:

$$y(k+j) = \frac{B(q^{-1})}{A(q^{-1})}u(k+j-1) + \frac{1}{A(q^{-1})\Delta}v(k+j) \tag{4}$$

The Diophantine equation is used to decompose the last term of relation (4):

$$\frac{1}{A(q^{-1})\Delta} = F_j(q^{-1}) + q^{-j}\frac{G_j(q^{-1})}{A(q^{-1})\Delta} \tag{5}$$

where $F_j(q^{-1})$ and $G_j(q^{-1})$ are polynomials defined as:

$$F_j(q^{-1}) = f_0 + f_1 q^{-1} + \cdots + f_{j-1} q^{-n_{F_j}} \tag{6}$$

$$G_j(q^{-1}) = g_{0j} + g_{1j} q^{-1} + \cdots + g_{n_{G_j}j} q^{-n_{G_j}} \tag{7}$$

The polynomial $F_j(q^{-1})$ is of degree $n_{F_j} = j - 1$, while $G_j(q^{-1})$ is of degree $n_{G_j} = n_A$.
Substituting (5) into (4), we obtain:

$$y(k+j) = \frac{B(q^{-1})}{A(q^{-1})}u(k+j-1) + F_j(q^{-1})v(k+j) + \frac{G_j(q^{-1})}{A(q^{-1})\Delta}v(k) \tag{8}$$

Combining (8) with the CARIMA model (3), the predictor becomes:

$$y(k+j) \quad = G_j(q^{-1})\,y(k) + B(q^{-1})F_j(q^{-1})\,\Delta u(k+j-1) + F_j(q^{-1})\,v(k+j) \tag{9}$$

To compute the j-step ahead predictor, the performance criterion is defined as:

$$J = \mathbb{E}\left\{\left(y(k+j) - \hat{y}(k+j)\right)^2\right\} \tag{10}$$

Since the noise sequence is assumed to be a zero-mean stochastic process with finite variance, the optimal prediction minimizing (10) is:

$$\hat{y}(k+j) = G_j(q^{-1})y(k) + B(q^{-1})F_j(q^{-1})\Delta u(k+j-1) \tag{11}$$

The term $B(q^{-1})F_j(q^{-1})$ is decomposed as:

$$B(q^{-1})F_j(q^{-1}) = Q_j(q^{-1}) + q^{-j}R_j(q^{-1}) \tag{12}$$

where $Q_j(q^{-1})$ and $R_j(q^{-1})$ are polynomials defined as:

$$Q_j(q^{-1}) \quad = q_0 + q_1 q^{-1} + \cdots + q_{j-1} q^{-n_{Q_j}} \quad \text{and} \quad R_j(q^{-1}) = r_{0j} + r_{1j} q^{-1} + \cdots + r_{n_{R_j}j} q^{-n_{R_j}} \tag{13}$$

The polynomial $Q_j(q^{-1})$ is of degree $n_{Q_j} = j - 1$, while $R_j(q^{-1})$ is of degree $n_{R_j} = n_B - 1$.

Submitted - May 2026; Final Version Received – July 2026; Accepted - July 2026; Published Online – July 2026

https://ajeat.org/ ISSN: XXXX - XXXX

Academic Journal of Engineering Applications (AJEA)
Volume: 1 Issue: 1, July 2026, pp. 38 – 51

c) Prediction Model in Matrix Form: For $j = 1,\ldots,H_p$, stacking all predictions leads to:

$$Y = N\Delta U + GY_p + R\Delta U_p \tag{14}$$

where:

$$\begin{aligned} Y &= \left[\hat{y}(k+1) \quad \cdots \quad \hat{y}(k+H_p)\right], \\ \Delta U &= [\Delta u(k) \quad \cdots \quad \Delta u(k+H_c-1)], \\ Y_p &= [y(k) \quad \cdots \quad y(k-n_A)], \\ \Delta U_p &= [\Delta u(k-1) \quad \cdots \quad \Delta u(k-n_B-1)]. \end{aligned}$$

The matrix N represents the influence of future control increments on the predicted output. The matrix has a lower triangular Toeplitz structure, given by:

$$N = \begin{bmatrix} q_0 & 0 & \cdots & 0 \\ q_1 & q_0 & \cdots & 0 \\ \vdots & \vdots & \ddots & \vdots \\ q_{H_p-1} & q_{H_p-2} & \cdots & q_{H_p-H_c} \end{bmatrix}, \quad N \in \mathbb{R}^{H_p \times H_c}$$

where H_p is the prediction horizon and H_c is the control horizon.

Each row corresponds to a future prediction step, and each column represents the effect of a control increment. The matrix G captures the influence of actual and past outputs values on the predicted output. It can be written as:

$$G = \begin{bmatrix} g_{01} & g_{11} & \cdots & g_{n_A1} \\ \vdots & \vdots & \ddots & \vdots \\ g_{0H_p} & g_{1H_p} & \cdots & g_{n_AH_p} \end{bmatrix}, \quad G \in \mathbb{R}^{H_p \times n_A}$$

where n_A is the order of the polynomial $A(q^{-1})$.

The matrix R represents the influence of past control inputs on the predicted output. In the general case, it can be written as:

$$R = \begin{bmatrix} r_{01} & r_{11} & \cdots & r_{n_B-11} \\ \vdots & \vdots & \ddots & \vdots \\ r_{0H_p} & r_{1H_p} & \cdots & r_{n_B-1H_p} \end{bmatrix}, \quad R \in \mathbb{R}^{H_p \times n_B}$$

where n_B is the order of the polynomial $B(q^{-1})$. Each row of R corresponds to a future prediction step, while each column reflects the contribution of past control increments.

Control Law Computation: The predictive control law is obtained by minimizing a quadratic cost function over the prediction horizon H_p. The objective is to compute the optimal control increments ΔU that ensure reference tracking while penalizing control effort. The cost function is defined as:

$$J = \sum_{j=1}^{H_p}\left(\hat{y}(k+j) - y_c(k+j)\right)^2 + \lambda \sum_{j=0}^{H_c-1}\left(\Delta u(k+j)\right)^2 \tag{15}$$

The cost function can be written in compact matrix form as:

$$J = (Y - Y_c)^T(Y - Y_c) + \lambda(\Delta U)^T(\Delta U) \tag{16}$$

where:

- Y: predicted output over the prediction horizon,
- Y_c: reference trajectory,

$$Y_c = \left[y_c(k+1) \quad \cdots \quad y_c(k+H_p)\right]$$

- ΔU: control increment sequence,
- λ: weighting factor for control effort.

Academic Journal of Engineering Applications (AJEA)
Volume: 1 Issue: 1, July 2026, pp. 38 – 51

Minimization of (16) with respect to ΔU gives:

$$\Delta U = L(Y_c - GY_p - R\Delta U_p) \tag{17}$$

where:

$$L = (N^T N + \lambda I)^{-1} N^T \tag{18}$$

Predictive Control Algorithm: The predictive control algorithm is implemented according to the following steps:

1) **Initialization**
   - Define model parameters $A(q^{-1})$, $B(q^{-1})$
   - Set the prediction horizon H_p, the control horizon H_c and the parameter λ.
   - Initialize system states and control input
2) **Offline Matrix Computation**
   - Compute the prediction matrices N, G, R and L
   - Construct the reference trajectory y_c
3) **At each time step k**
   - **Theoretical model:** The system is described by the following difference equation:

$$y(k) = -\sum_{i=1}^{n_A} a_i\, y(k-i) + \sum_{i=0}^{n_B} b_i\, u(k-i-1) \tag{19}$$

   - Build past state vectors Y_p and ΔU_p and the vector Y_c
   - Compute control increment:

$$\Delta U = L(Y_c - GY_p - R\Delta U_p) \tag{20}$$

   - Update control signal:

$$u(k) = u(k-1) + \Delta U(1,1) \tag{21}$$

After completing the iterative procedure over all time steps k, the system performance is evaluated. The output signal $y(k)$ is plotted and compared with the reference signal $y_c(k)$ to assess the tracking capability.

III. SYSTEM DESCRIPTION AND MODEL IDENTIFICATION

A. Hardware Components

The experimental temperature regulation system, shown in Figure 1, integrates four primary hardware components: the ESP32-S3 mini microcontroller, a DHT22 temperature sensor, an AC dimmer module, and a 220 V AC incandescent lamp used as the heating element. The lamp behaves as a resistive load and is installed inside a wooden enclosure, which acts as a controlled thermal chamber and provides partial thermal insulation for the experiments. Each component has been selected based on its functionality, ease of integration, and suitability for real-time temperature control in a hydroponic environment.

The ESP32-S3 mini development board used in this work is a compact and high-performance microcontroller module based on the ESP32-S3 system-on-chip (SoC). It features a dual-core Xtensa® LX7 processor operating at a frequency of up to 240 MHz, providing sufficient computational power for real-time control applications such as PI and predictive control algorithms [14]. The board integrates 512 KB SRAM, 384 KB ROM, 4 MB of Flash memory, and 2 MB of PSRAM, allowing efficient data processing and storage for embedded applications. It supports 2.4 GHz Wi-Fi (802.11 b/g/n) and Bluetooth 5 (Low Energy), enabling wireless communication and remote monitoring capabilities in hydroponic systems [14].

In terms of hardware interfaces, the ESP32-S3 mini provides multiple communication peripherals, including SPI, I^2C, UART, and ADC channels, as well as up to 24 configurable GPIO pins. These interfaces are used to connect the DHT22 temperature sensor and control the AC dimmer module. The board also includes a USB Type-C interface for programming and power supply, simplifying system integration.

Additionally, the ESP32-S3 incorporates advanced features such as hardware encryption, random number generation (RNG), and low-power operating modes, making it suitable for IoT-based monitoring and control systems. Its flexibility,

Submitted - May 2026; Final Version Received – July 2026; Accepted - July 2026; Published Online – July 2026

https://ajeat.org/ ISSN: XXXX - XXXX

Academic Journal of Engineering Applications (AJEA)
Volume: 1 Issue: 1, July 2026, pp. 38 – 51

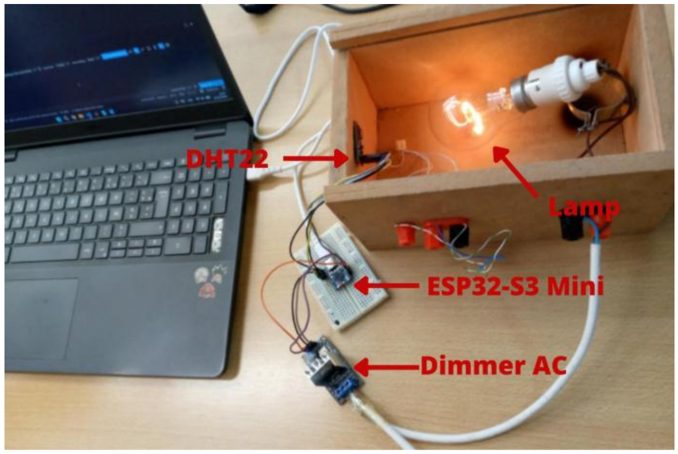

Figure 1 Experimental prototype setup.

processing capability, and integrated connectivity make it an ideal choice for implementing a closed-loop temperature regulation system in hydroponic environments [14].

The DHT22 is a low-cost, digital temperature and humidity sensor widely used for environmental monitoring in embedded systems [12]. It communicates via a single-wire digital interface, which simplifies integration with microcontrollers like the ESP32-S3.

Key characteristics include:

- Temperature range: -40°C to 80°C
- Temperature accuracy: $\pm 0.5^\circ$C
- Digital output: single-wire communication
- Supply voltage: typically 3.0 V to 5.5 V
- Resolution: programmable from 9 to 12 bits
- Low power consumption

The wiring of the DHT22 sensor is straightforward and requires three main connections: VCC, GND, and DATA. The sensor operates typically at 3.3 V or 5 V, where the VCC pin is connected to the power supply of the ESP32-S3, and the GND pin is connected to the common ground. The DATA pin is connected to a digital GPIO pin of the microcontroller [15], [16].

In this system, the DHT22 provides continuous temperature readings from the hydroponic environment. The ESP32-S3 reads these values at regular intervals and uses them as feedback for the control algorithm. Although the DHT22 has moderate accuracy, it is suff icient for educational and prototyping purposes.

An AC dimmer is used as the actuator interface to control the thermal load in the hydroponic system. The dimmer adjusts the voltage applied to a resistive heater or other thermal element, effectively modulating its power and controlling the temperature [13].

The power supplied to the heating element is continuously adjusted based on the temperature measurements provided by the DHT22 sensor, enabling closed-loop regulation of the thermal environment.

Key features of the AC dimmer module include:

- Input voltage: 220–240 VAC
- Load type: resistive (AC lamp used as heater)
- Control method: phase-angle control using TRIAC
- Zero-crossing detection for synchronization with AC signal
- Control input: digital signal from ESP32-S3 (PWM or delay-based triggering)

The ESP32-S3 generates a control signal based on the difference between the measured temperature and the desired setpoint. This signal determines the phase angle at which the dimmer activates the AC supply to the heater, providing

https://ajeat.org/ ISSN: XXXX - XXXX

Academic Journal of Engineering Applications (AJEA)
Volume: 1 Issue: 1, July 2026, pp. 38 – 51

smooth and proportional temperature control. Using phase-angle control minimizes thermal overshoot and improves energy eff iciency compared to simple on/off switching.

For system integration, the ESP32-S3, the DHT22 sensor, and the AC dimmer form a closed-loop temperature control system. The DHT22 measures the current temperature inside the thermal chamber, the ESP32-S3 computes the control action using either a PI or predictive control algorithm, and the AC dimmer regulates the power delivered to the 220 V AC incandescent lamp in order to maintain the desired temperature setpoint.

B. Architecture of the Temperature Regulation System

The proposed temperature regulation system is based on a closed-loop control architecture designed to maintain a desired thermal condition for hydroponic crops. As illustrated in Figure 2, the system operates through three main stages: measurement, control, and actuation.

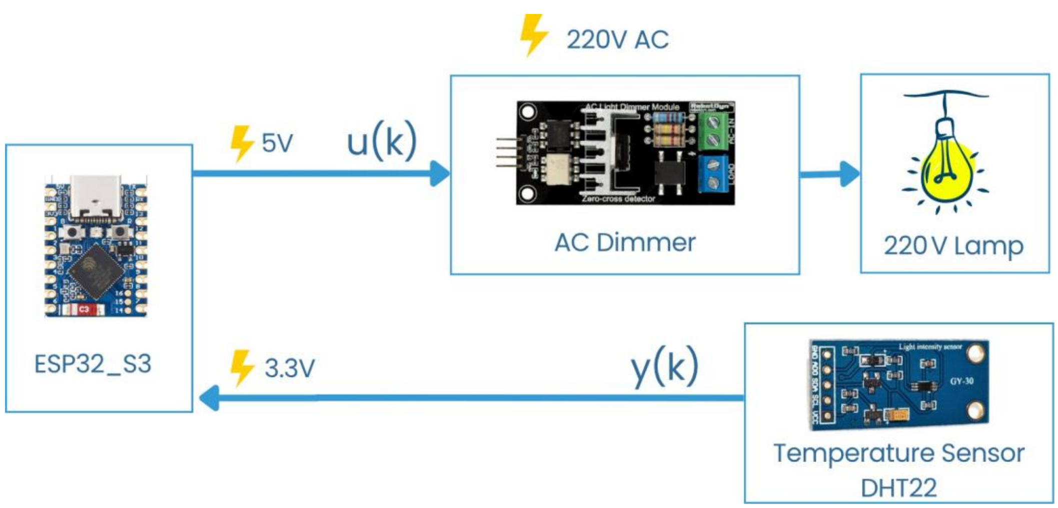

Figure 2 Architecture of the temperature regulation system.

First, the ambient temperature inside the hydroponic enclosure is measured using a DHT22 temperature sensor. The measured value is then transmitted to the ESP32-S3 microcontroller, where it is processed in real time. The controller computes the appropriate control action in order to minimize the error between the measured temperature and the desired reference (setpoint), using control strategies such as Proportional-Integral (PI) and predictive control.

Finally, the control signal drives the thermal actuator through an AC dimmer module that adjusts the power supplied to the heating element (220 V AC lamp). By regulating the power delivered to the lamp, the system is able to maintain the desired temperature within the hydroponic environment.

C. Model Identification

Principle of the Recursive Least Squares Method: The objective of this step is to identify a mathematical model of the system from experimental data in order to predict its dynamic response. For this purpose, the Recursive Least Squares (RLS) method, suitable for discrete linear systems, was used. It consists of adjusting the coeff icients of a model to minimize the quadratic error between the measured output $y(k)$ and the predicted output $\hat{y}(k)$ of the model. This approach is particularly appropriate for systems whose dynamics can be approximated by linear models.

RLS Algorithm: The principle is based on recursively updating the model coeff icients at each new sample. The initial covariance matrix is defined as $P_0 = (10^{\alpha})I_n$ where α is a large positive constant ensuring high initial adaptation gain and $n = n_A + n_B + 1$. For a general model of orders n_A and n_B, the parameter vector is defined as:

$$\theta = [a_1 \quad a_2 \quad \cdots \quad a_{n_A} \quad b_0 \quad b_1 \quad \cdots \quad b_{n_B}]^T \tag{22}$$

Submitted - May 2026; Final Version Received – July 2026; Accepted - July 2026; Published Online – July 2026

https://ajeat.org/ ISSN: XXXX - XXXX

Academic Journal of Engineering Applications (AJEA)
Volume: 1 Issue: 1, July 2026, pp. 38 – 51

This vector θ is initialized to zero and updated at each iteration. The regression vector is given by:

$$h(k)^T = [-y(k-1) \cdots -y(k-n_A) \quad u(k-1) \cdots u(k-n_B-1)] \tag{23}$$

The model output can be written as:

$$\hat{y}(k) = h(k)^T \, \theta(k-1) \tag{24}$$

At each time step k, the following updates are performed:
The adaptation gain is then computed as:

$$G(k) = \frac{P(k-1)h(k)}{1 + h(k)^T P(k-1)h(k)}.$$

and the parameter update follows:

$$\theta(k) = \theta(k-1) + G(k)\big(y(k) - \hat{y}(k)\big).$$

Finally, the covariance matrix is updated at each iteration:

$$P(k) = P(k-1) - G(k)h(k)^T P(k-1).$$

The model performance is then evaluated using the mean error:

$$v_1 = \sum_{i=1}^{N}\big(y(k) - \hat{y}(k)\big)^2 \tag{25}$$

To determine the system model, open-loop experiments were conducted. The used input signal and the measured output signal obtained from the real system, with a sampling time $T_e = 2$ s, are shown in Figure 3 and Figure 4, respectively.

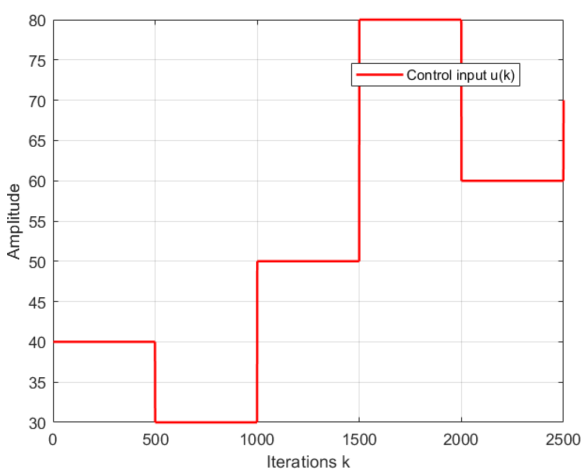

Figure 3 Input signal $u(k)$ used for system identification.

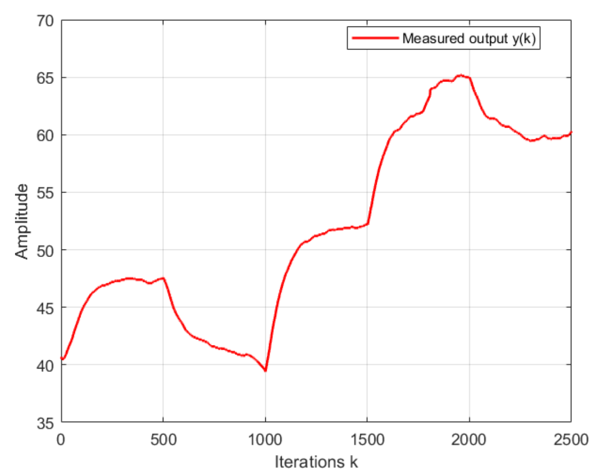

Figure 4 Measured output signal $y(k)$ of the system.

For parameter estimation, the data set corresponding to $k = 1$ to 1500 was used. The remaining data, from $k = 1501$ to 2500, was used for model validation.
The model parameters were identified using the Recursive Least Squares (RLS) method.
Based on the first 1500 measurements, the estimated parameters for the different model orders are summarized in Table I.

Submitted - May 2026; Final Version Received – July 2026; Accepted - July 2026; Published Online – July 2026

https://ajeat.org/ ISSN: XXXX - XXXX

Academic Journal of Engineering Applications (AJEA)
Volume: 1 Issue: 1, July 2026, pp. 38 – 51

TABLE I: Estimated model parameters using RLS method.

Model	a_1	a_2	a_3	b_0	b_1	b_2
Model 1	-0.9701	–	–	0.0344	–	–
Model 2	-0.8037	-0.1923	–	-0.0040	0.0087	–
Model 3	-0.8447	-0.3547	0.2025	-0.0038	0.0103	-0.0027

To further analyze the identification process, the evolutions of the estimated parameters are illustrated in Figure 5, Figure 6, and Figure 7 for the first-, second-, and third-order models, respectively.

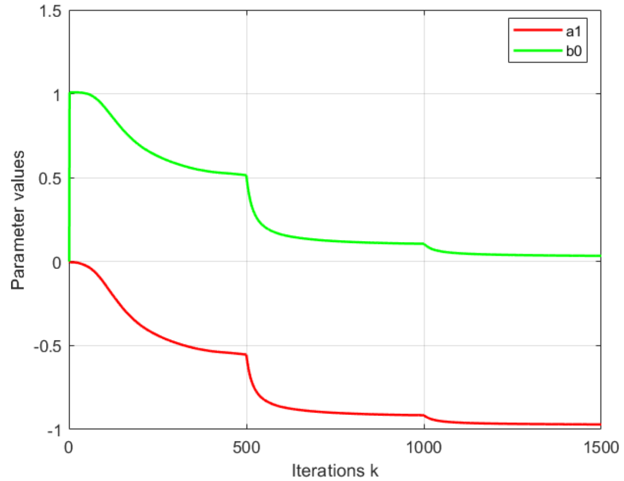

Figure 5 Evolution of parameters for the first-order model.

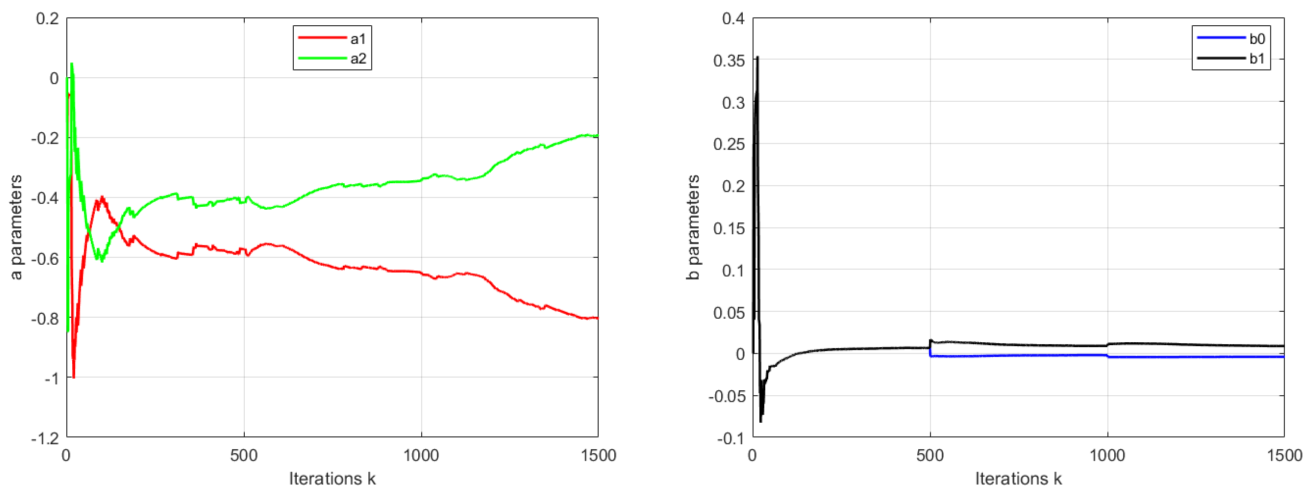

Figure 6 Evolution of parameters for the second-order model.

Submitted - May 2026; Final Version Received – July 2026; Accepted - July 2026; Published Online – July 2026

Academic Journal of Engineering Applications (AJEA)
Volume: 1 Issue: 1, July 2026, pp. 38 – 51

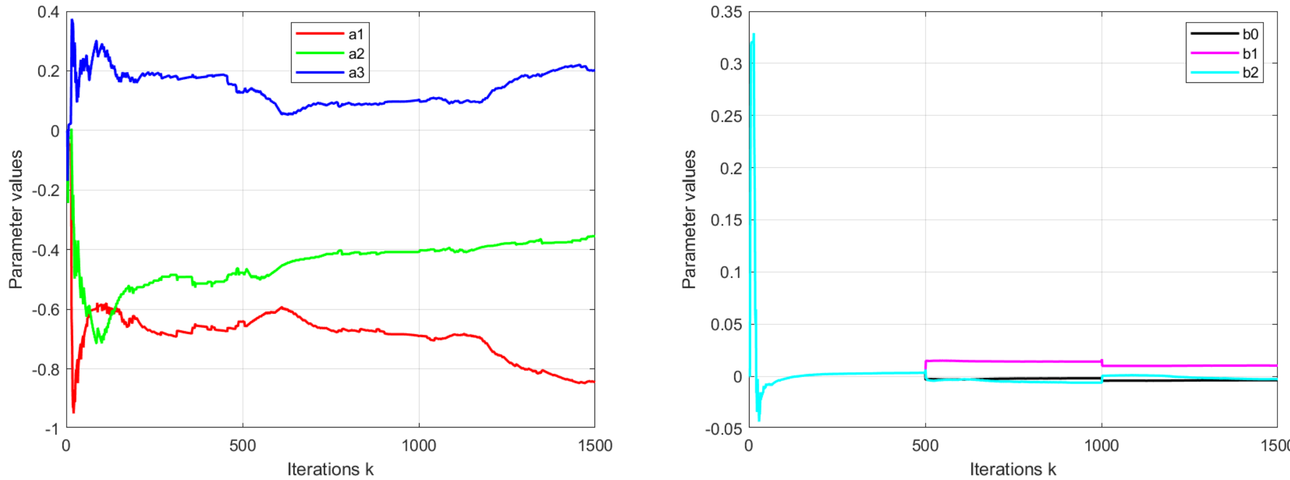

Figure 7 Evolution of parameters for the third-order model.

These figures highlight the convergence behavior of the RLS algorithm and provide insight into the stability and dynamics of the identified models.

It can be observed that the parameters converge progressively towards steady-state values, with faster convergence for the lower-order model and more complex transient behavior as the model order increases.

To evaluate the accuracy of the identified models, the Mean Squared Error (MSE) is computed over the validation data set, corresponding to $k = 1501$ to 2500. The general expression of the criterion is given by:

$$J = 10^{-3} \sum_{k=1501}^{2500} \big(y(k) - \hat{y}(k)\big)^2 \tag{26}$$

where N is the number of validation samples.

The obtained values of the quadratic error for the different model orders are summarized in Table II.

TABLE II: Mean squared error for different model orders.

Model	J
First-order model	3.6874
Second-order model	4.9647
Third-order model	6.6023

Model Selection: Although the first-order model yields the lowest mean squared error on the validation data, it provides a simplified representation of the system dynamics. In contrast, higher-order models are able to capture more complex dynamic behaviors.

The third-order model, despite its increased flexibility, exhibits a higher prediction error, which may indicate overfitting and reduced generalization capability.

Therefore, a trade-off between model accuracy and complexity is considered. The second-order model offers a good compromise, providing an adequate representation of the system dynamics while maintaining a reasonable prediction error.

For this reason, the second-order model is selected for the design of the predictive controller in the following section.

IV. EXPERIMENTAL RESULTS

This section presents the experimental evaluation of the proposed temperature regulation system using a PI controller and a predictive controller. The performance of each control strategy is analyzed under different operating conditions, including scenarios with and without disturbances.

Submitted - May 2026; Final Version Received – July 2026; Accepted - July 2026; Published Online – July 2026

https://ajeat.org/ ISSN: XXXX - XXXX

Academic Journal of Engineering Applications (AJEA)
Volume: 1 Issue: 1, July 2026, pp. 38 – 51

A. Experimental Conditions

The experiments were conducted using the developed prototype. The objective is to regulate the measured temperature $y(k)$ to follow a desired reference $y_c(k)$.

A step reference signal is applied to evaluate the dynamic response of the system. In addition, external disturbances are introduced to assess the robustness of each controller.

B. System Responses to Step Temperature Reference

The system response to a step reference signal was evaluated using both the PI controller and the predictive controller.

a) PI Controller Response: Figure 8 shows the reference temperature, the measured output, and the control input obtained with the PI controller. The controller parameters were selected as:

$$c_0 = 0.02, \quad c_1 = 0.001.$$

From Figure 8, it can be observed that the measured temperature follows the reference signal with acceptable accuracy, indicating that the controller ensures stable regulation under nominal conditions.

A slight overshoot is noticeable at the beginning of the transient phase, which is typical of PI-controlled thermal systems due to the integral action. Small oscillations around the setpoint are also observed. These behaviors are strongly influenced by the tuning of the controller parameters c_0 and c_1, which affect the overall dynamic performance, including rise time, overshoot, and stability.

The control input exhibits significant peaks and oscillations, reflecting a relatively aggressive control action.

Overall, the PI controller provides a satisfactory trade-off between stability and performance for slow thermal dynamics, although its performance remains highly dependent on parameter tuning.

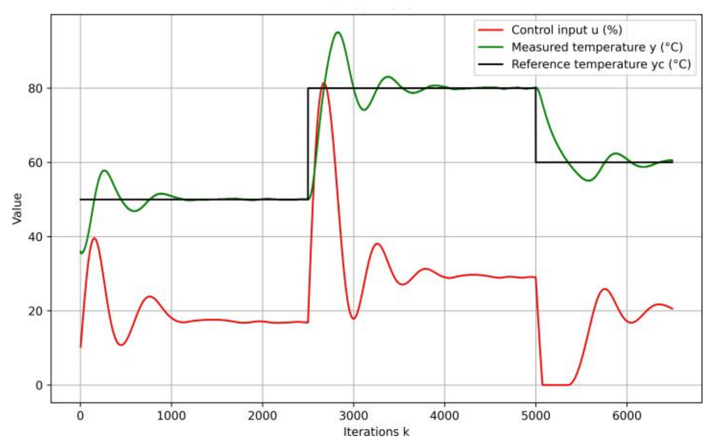

Figure 8 PI controller response without perturbation.

b) Predictive Controller Response: After implementing the predictive control algorithm described in section II-B, equation 19 is replaced by the measured output $y(k)$, and the control input is computed accordingly. At the end of each iteration of the algorithm loop, the control input is applied to the system.

Figure 9 presents the system response obtained using the predictive controller under the same operating conditions. It can be observed that the measured temperature follows the reference signal with satisfactory accuracy. The PI controller shows a noticeable overshoot, exceeding the desired setpoint during the transient phase, while the predictive controller provides a more controlled response. Nevertheless, both controllers converge to the steady-state at the same time, around 4000 sampling instants.

Despite this similar convergence speed, the predictive controller exhibits improved behavior in terms of control effort. The control input is smoother and does not present significant peaks or oscillations, in contrast to the PI controller. This reflects a more refined and less aggressive control action.

Submitted - May 2026; Final Version Received – July 2026; Accepted - July 2026; Published Online – July 2026

https://ajeat.org/ ISSN: XXXX - XXXX

Academic Journal of Engineering Applications (AJEA)
Volume: 1 Issue: 1, July 2026, pp. 38 – 51

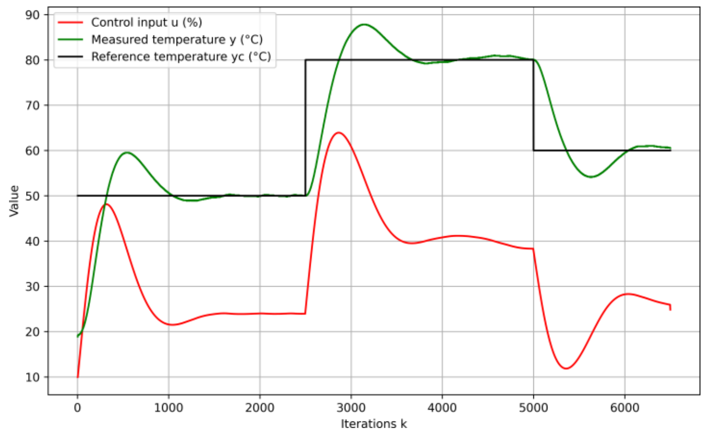

Figure 9 Predictive controller without perturbation.

The performance of the predictive controller is strongly influenced by the tuning parameters, namely the prediction horizon h_p, the control horizon h_c, and the weighting factor λ. These parameters determine the trade-off between tracking performance and control effort.

These characteristics highlight the ability of the predictive controller to better handle system dynamics by anticipating future behavior, leading to improved control signal quality while maintaining acceptable tracking performance. Overall, although the predictive controller does not enhance the response speed, it provides a more stable and smoother control input, which can be advantageous for thermal systems where actuator limitations and energy efficiency are important considerations.

C. Response under Perturbation

To evaluate the robustness of the temperature regulation system, external disturbances were introduced while the controllers were operating. Both the PI and predictive controllers were tested under the same perturbation scenarios. The objective is to observe how well each controller maintains the temperature at the desired set-point despite disturbances.

1) PI Controller Response: Figure 10 shows the temperature output $y(k)$, the control signal $u(k)$, and the reference temperature $y_c(k)$ under perturbation using the PI controller. The results demonstrate that the system response under

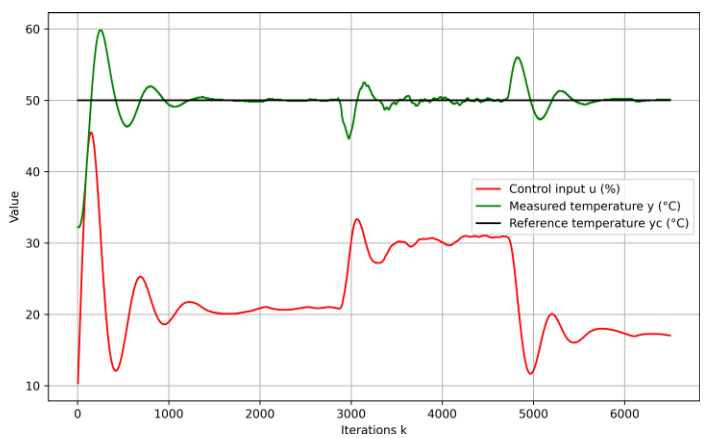

Figure 10 PI controller response under perturbation.

perturbation when using the PI controller. The measured temperature remains close to the reference, indicating that the controller is able to ensure acceptable regulation despite the presence of disturbances.

Submitted - May 2026; Final Version Received – July 2026; Accepted - July 2026; Published Online – July 2026

https://ajeat.org/ ISSN: XXXX - XXXX

Academic Journal of Engineering Applications (AJEA)
Volume: 1 Issue: 1, July 2026, pp. 38 – 51

However, small oscillations are observed around the setpoint following the disturbance, reflecting the sensitivity of the PI controller to external variations. These oscillations are also related to the tuning of the controller parameters, which influence the damping and dynamic response.

In terms of control effort, the input signal exhibits noticeable oscillations, indicating a fluctuating and relatively reactive control action. Although the PI controller maintains stability and acceptable tracking performance, its response is characterized by oscillatory behavior in both the output and the control input.

2) Predictive Controller Response: Figure 11 presents the system response under perturbation when using the predictive controller. The output remains close to the reference, showing that the controller ensures satisfactory regulation under disturbed conditions, with a convergence time comparable to that of the PI controller.

Unlike the PI controller, the predictive approach exhibits a noticeable peak in the output at the moment of disturbance, indicating a more pronounced transient response. However, the oscillations around the setpoint are reduced afterward.

Regarding the control input, the predictive controller produces a smoother signal without oscillations, although with larger amplitude variations. This reflects a more structured and anticipative control strategy, governed by the tuning parameters h_p, h_c, and λ.

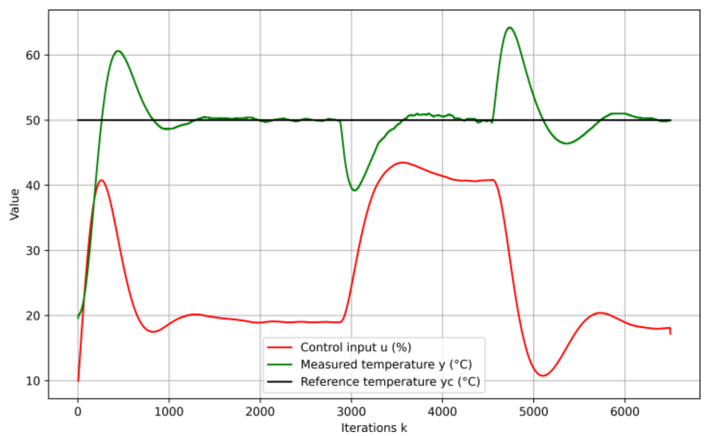

Figure 11 Predictive controller response under perturbation.

Overall, both controllers are able to maintain the temperature close to the reference under perturbation, with similar convergence times. The PI controller provides a more damped output response with smaller peaks but introduces oscillations in both the output and control input.

In contrast, the predictive controller generates a smoother control signal with reduced oscillations, at the expense of a larger transient peak in the output. This highlights a trade-off between control smoothness and transient behavior, which depends on the tuning of the respective controller parameters.

V. CONCLUSION

This work presented the design and experimental evaluation of a temperature regulation system using PI and predictive controllers. The experimental results demonstrate that both controllers are capable of maintaining the desired temperature under normal operating conditions. The PI controller exhibits faster response but with more pronounced oscillations. In contrast, the predictive controller shows a larger overshoot but provides a smoother response with fewer oscillations.

The PI and predictive controllers were further tested under external perturbations. Results show that both controllers can compensate for disturbances, with the predictive controller exhibiting smaller deviations from the reference and smoother control actions.

Overall, the study confirms that predictive control offers superior performance in terms of response speed and robustness to disturbances, whereas the PI controller remains simple and effective for practical implementation. Both strategies enable reliable temperature regulation, ensuring consistent system performance under varying operating conditions.

Submitted - May 2026; Final Version Received – July 2026; Accepted - July 2026; Published Online – July 2026

REFERENCES

[1] N. N. Venkatasai, D. N. Shetty, C. M. Vinay et al., "A comprehensive review of factors affecting growth and secondary metabolites in hydroponically grown medicinal plants", *Planta*, vol. 261, no. 48, Jan. 2025. DOI: 10.1007/s00425-025-04619-y.
[2] P. Sharma, A. K. Singh, A. Raushan, Shubham, and S. Kaushal, "Influence of artificial lighting on plant growth in hydroponic environments", *Journal of Scientific Research and Reports*, vol. 31, no. 5, pp. 116–125, 2025. DOI: 10.9734/jsrr/2025/v31i53009.
[3] J. Yang, J. Sun, X. Wang, and B. Zhang, "Light intensity affects growth and nutrient value of hydroponic barley fodder", *Agronomy*, vol. 14, no. 6, p. 1099, 2024. DOI: 10.3390/agronomy14061099.
[4] K. Exaudi, S. Sembiring, A. Prasetyo, D. Stiawan, H. Fakhrurroja, and R. Budiarto, "Innovative smart showcase design for indo ors and eco-friendly hydroponics", *Bulletin of Electrical Engineering and Informatics*, vol. 14, no. 4, pp. 2912–2922, Aug. 2025. DOI: 10.11591/eei.v14i4.8353.
[5] U. Shareef, A. U. Rehman, and R. Ahmad, "A Systematic Literature Review on Parameters Optimization for Smart Hydroponic Systems", *AI*, vol. 5, pp. 1517–1533, 2024. DOI: 10.3390/ai5030073.
[6] M. Rathedi, O. Matsebe, and N. M. J. Ditshego, "Performance Evaluation of Hydroponics Control Systems for pH, Temperature, an d Water Level Control", *International Journal of Engineering Research in Africa*, vol. 65, pp. 105–116, 2023. DOI: 10.4028/p-RBT3yU.
[7] S. Wahyuni, A. Rusydi, and M. Fuad, "Hydroponic NFT Agricultural Monitoring: Temperature Control Based on PID", in *BIO Web of Conferences*, 2024, p. 01096. DOI: 10.1051/bioconf/202414601096.
[8] Y. Cai, Z. Zhao, W. Guo, H. Xu, Y. Teng, X. Han, Q. Zhao, and L. Wang, "Smart Nutrient Solution Temperature Control System for Oversummering Lettuce Cultivation Based on Adaptive Dung Beetle Optimizer–Fuzzy PID", *Applied Sciences*, vol. 15, p. 5381, 2025. DOI: 10.3390/app15105381.
[9] J. Qin and S. Badgwell, "Model Predictive Control and its Application in Agriculture: A Review", *Computers and Electronics in Agriculture*, vol. 151, pp. 104–117, 2018. DOI: 10.1016/j.compag.2018.06.004.
[10] E. Bwambale et al., "A Review of Model Predictive Control in Precision Agriculture", *Smart Agricultural Technology*, vol. 10, p. 100716, 2025. DOI: 10.1016/j.atech.2024.100716.
[11] H. Hamidane, S. El Faiz, M. Guerbaoui, A. Ed-Dahhak, A. Lachhab, and B. Bouchikhi, "Constrained Discrete Model Predictive Control of a Greenhouse System Temperature", *International Journal of Electrical and Computer Engineering*, vol. 11, p. 1223, 2021.
[12] P. Adalimum and S. Kumar, "Temperature and Humidity Monitoring Using DHT22 Sensor", *International Journal of Advanced Research in Electronics and Communication Engineering*, vol. 6, no. 8, pp. 85–89, 2017.
[13] N. Mohan, T. M. Undeland, and W. P. Robbins, *Power Electronics: Converters, Applications, and Design*, 4th ed., Wiley, 2019.
[14] OceanLabz, "Getting Started with ESP32-S3 Mini Development Board", 2025. [Online]. Available: https://www.oceanlabz.in/getting-started-with-esp32-s3-mini-development-board/ [Accessed: Apr. 25, 2026].
[15] Aosong Electronics, "DHT22 Temperature and Humidity Sensor Datasheet", 2018.
[16] Arduino, "DHT22 Digital Temperature and Humidity Sensor – Interfacing Guide", Arduino Documentation, 2022.
[17] D. Thakulla et al., "Nutrient Solution Temperature Affects Growth and Brix Parameters of Lettuce Cultivars in Hydroponics", *Horticulturae*, vol. 7, no. 9, p. 321, 2021. DOI: 10.3390/horticulturae7090321.

Submitted - May 2026; Final Version Received – July 2026; Accepted - July 2026; Published Online – July 2026